ACS APPLIED MATERIALS & INTERFACES

Research Article

www.acsami.org

Surface Transfer Doping of Cubic Boron Nitride Films by MoO_3 and Tetrafluoro-tetracyanoquinodimethane (F4-TCNQ)

Bin He, Tsz-Wai Ng, Ming-Fai Lo, Chun-Sing Lee, and Wenjun Zhang*

Center of Super-Diamond and Advanced Films (COSDAF), and Department of Physics and Materials Science, City University of Hong Kong, Hong Kong SAR, P.R. China

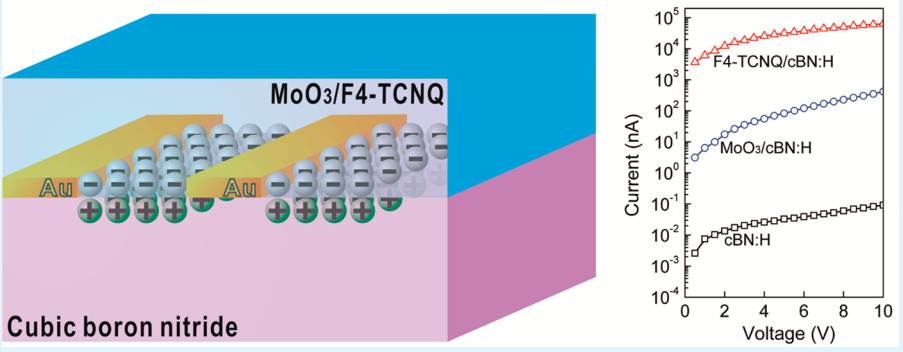

ABSTRACT: Cubic boron nitride (cBN) has strong potential for the applications in high-temperature and high-power electronics and deep ultraviolet devices due to its outstanding combined physical and chemical properties. P-type surface transfer doping of heteroepitaxial cBN films was achieved by employing MoO_3 and tetrafluoro-tetracyanoquinodimethane (F4-TCNQ) as the surface dopants. The surface conductivities of hydrogenated cBN films increased by 3−6 orders after the deposition of surface dopants. The photoemission spectroscopy (PES) measurements revealed the variation of electronic structures at the interface regions, which suggested that the electron transfer from cBN films to the surface dopants induced hole accumulation at the cBN surface and the increase of surface conductivity. Based on the PES results, the energy level diagrams at MoO_3/cBN and F4-TCNQ/cBN interfaces were determined. The achievement provided a potential approach for fabricating cBN-based electronic devices, especially on micrometer and nanometer scales.

KEYWORDS: *cubic boron nitride (cBN), surface transfer doping, photoemission spectroscopy (PES), band bending, interface dipole, electronic structure*

INTRODUCTION

Cubic boron nitride (cBN), an isostructural and isoelectronic material of diamond, has great potentials for applications in high-temperature and high-power electronics and deep ultraviolet (DUV) devices due to its large band gap (6−6.4 eV, the largest among all covalent materials), high hardness, high thermal conductivity (13 W/(cm K)), large breakdown field strength (8×10^6 V/cm), and high thermal stability.[1] These outstanding properties make cBN attractive for the fabrication of electronic devices enabling to operate in harsh environments. A prerequisite for realizing cBN-based electronic devices is the capability to understand and control its electronic and transport properties through doping processes. Based on the high-pressure high-temperature (HPHT) processes,[2] p- and n-type cBN single crystals were synthesized by incorporating impurities such as Be, Mg, Si and S.[3] Significantly, high-temperature cBN p−n junctions and DUV light-emitting diodes (LEDs) have also been demonstrated.[4−6] However, the HPHT method can only produce crystallites with limited size ranging from micrometers to millimeters, which obstructs the electronic applications of cBN.

Various physical and chemical vapor deposition (PVD and CVD) techniques have been developed to grow cBN films.[7] Large-area cBN thin films with high quality and in particular heteroepitaxial cBN films have been achieved by using fluorine-assisted CVD[8] and ion-beam-assisted deposition.[9] Nevertheless, there have been thus far only a few work studying the doping process and electronic properties of cBN films.[1,10] Mg,[11] Zn,[12,13] and Si[14] were incorporated during the PVD processes to dope cBN films. p-type conduction was observed for Mg- and Zn-doped cBN films, however, the increase in conductivity was accompanied by a deviation from BN stoichiometry, suggesting that the p-type conduction was induced by the increased B/N ratio. The resistance of Si-doped cBN films decreased by 2 orders compared with undoped ones, however, the conduction type could not be determined due to the still high resistivity. Ion implantation followed by high-temperature annealing was also employed to dope cBN films,[15,16] n- and p-

Received: March 2, 2015
Accepted: April 27, 2015
Published: April 27, 2015

DOI: 10.1021/acsami.5b01779
ACS Appl. Mater. Interfaces 2015, 7, 9851−9857

type cBN films were achieved by Si and Be implantation, respectively.

An alternative approach to manipulate the electrical properties of semiconductor thin films is through surface transfer doping mechanism.[17,18] As the surface adsorbate has a misaligned Fermi level (E_F) with respect to that of the underlying thin film, electrons will be extracted from or injected into the thin film,[19] forming an electron-deficiency or electron-rich surface layer. Surface transfer doping has been widely accepted for interpreting the surface conductivity of hydrogenated diamond in air[20,21] and it has also been observed at Si/SiO_2 interface.[22] Recently, the surface transfer doping has been applied successfully to a variety of materials such as diamond,[23−27] graphene,[28−30] and silicon[31−33] to control their surface conductivities and electronic structures. It has been demonstrated that the efficiency of surface transfer doping for a semiconductor depends on its surface electronic structure and the selection of proper surface dopants.

In this work, we report the study on surface transfer doping of cBN films for the first time. Cubic BN with hydrogen-terminated surface (cBN:H) shows a negative electron affinity (NEA),[34−36] similar to hydrogenated diamond,[37,38] which strongly favors electrons to escape from the surface and makes it particularly susceptible to be p-type doped by surface transfer doping. Therefore, MoO_3 and tetrafluoro-tetracyanoquinodimethane (F4-TCNQ), which have large EAs (6.7 eV[27] and 5.2 eV,[24] respectively) in contrast to the NEA of cBN:H, were employed as surface acceptors to achieve p-type conduction on cBN films. The variations in the surface conductivity of cBN films induced by MoO_3 and F4-TCNQ layers were studied comparatively, and electronic structures at the surface of pristine cBN:H films and the MoO_3/cBN and F4-TCNQ/cBN interfaces were deduced to further illustrate the electron transfer and formation of interface dipoles.

EXPERIMENTAL PROCEDURES

The cBN films employed in this work were deposited in an ASTeX electron cyclotron resonance microwave plasma CVD (ECR MPCVD) system, and the experimental details have been reported elsewhere.[8,39,40] The substrates for cBN growth were diamond films coated Si wafers. The phase purity and the morphology of cBN films were characterized by Fourier transform infrared spectroscopy (FTIR) and scanning electron microscope (SEM), respectively.

Before the deposition of surface dopants, cBN films were pretreated by microwave hydrogen (H)-plasma at 800 °C and annealed at 400 °C at 1×10^{-6} Torr to obtain a hydrogenated surface with NEA.[35,36] For measuring the surface conductivity of cBN films, patterned electrodes of 1×1 mm^2 Au squares spaced by 50 μm from each other were thermally evaporated on the specimens. MoO_3 and F4-TCNQ were then thermally evaporated onto the cBN films with a thickness of 10 nm. The surface conductivity was determined by the current−voltage (I−V) characteristics between two adjacent contacts with an applied voltage from −10 to 10 V. Two control experiments were performed on the as-grown cBN films (without any H-plasma pretreatment) and a thermal SiO_2 layer on Si substrate.

The electronic structures at the MoO_3/cBN and F4-TCNQ/cBN interfaces were probed by photoemission spectroscopy (PES) measurements, including ultraviolet photoemission spectroscopy (UPS) and X-ray photoemission spectroscopy (XPS). The measurements were carried out in a VG ESCALAB 220i-XL UHV surface analysis system with a base pressure of 1×10^{-10} Torr. A He-discharge lamp (21.22 eV) and a monochromatic Al Kα X-ray (1486.6 eV) sources were equipped for UPS and XPS respectively. The instrumental energy resolution is 0.09 eV as estimated from the Fermi edge of a cleaned Au film. The samples were negatively biased at 5.0 V with respect to ground to overcome the work function difference between the analyzer and the samples. The Fermi edge was calibrated from a UPS spectrum using cleaned Au substrate. MoO_3 or F4-TCNQ was thermally evaporated onto cBN surface in a deposition chamber connected with the analysis system. The thickness was detected by a quartz crystal monitor installed in the deposition chamber. The XPS and UPS spectra were in situ acquired without breaking the vacuum after each evaporation step. The final thicknesses of MoO_3 and F4-TCNQ coatings were 20 and 5 nm, respectively.

RESULTS AND DISCUSSION

Figure 1 shows the cross-sectional SEM image of a typical cBN film with the thickness around 500 nm. The sharp peak at 1076

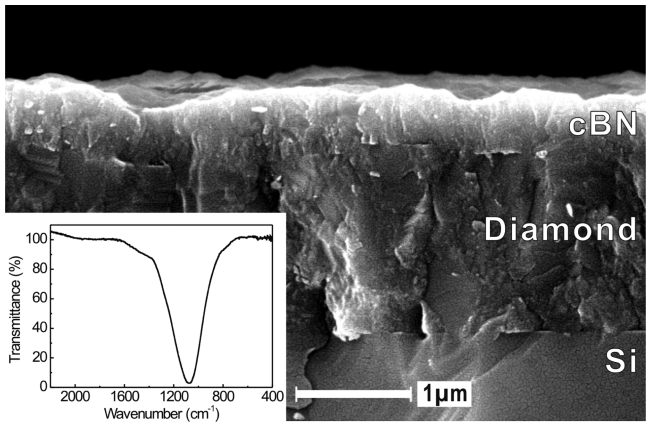

Figure 1. Cross-sectional SEM image of a cBN film on diamond coated silicon substrate. The corresponding FTIR spectrum in the inset indicates the high phase purity of the film.

cm^{-1} in the FTIR spectrum (the inset in Figure 1) is assigned to the transverse optical phonon mode of cBN, indicating the high phase purity of the film.[7] The deposition with fluorine-assisted CVD yields cBN films with higher crystallinity and much less defects than cBN produced by PVD techniques using relatively large bias for growth,[41] and the employment of diamond substrates enables the direct/epitaxial growth of cBN without any noncubic BN (turbostratic BN and amorphous BN) interlayer,[8] which are essential for the preparation of high-quality cBN films for electronic applications. Furthermore, the noncubic BN layer, which commonly existed on the surface of cBN films prepared by PVD methods,[41,42] was not observed here. A surface with pure cubic phase is essential for this study because the influences of noncubic phase BN impurities on the surface electronic structures have to be excluded.

Different from hydrogenated diamond, the cBN:H films did not show observable enhanced conductivity in air. However, after the deposition of MoO_3 and F4-TCNQ layers, the surface resistance of cBN:H films decreased significantly. Figure 2 shows the representative I−V characteristics measured before and after the deposition of surface dopants. The linear curves indicated the Ohmic contact between Au electrodes and cBN films. From the I−V curves, the surface resistance decreased by 3−4 orders after the deposition of MoO_3, and decreased even more by 4−6 orders for the samples coated with F4-TCNQ. Two control experiments were performed on the as-grown cBN films without any pretreatment and a thermal SiO_2 layer on Si substrate. Neither F4-TCNQ nor MoO_3 coatings could give any rise to the measured current.

The cBN films used for XPS and UPS measurements were grown on B-doped diamond coated Si substrates and Si ion implantation was employed to dope the cBN films.[16] A

DOI: 10.1021/acsami.5b01779
ACS Appl. Mater. Interfaces 2015, 7, 9851−9857

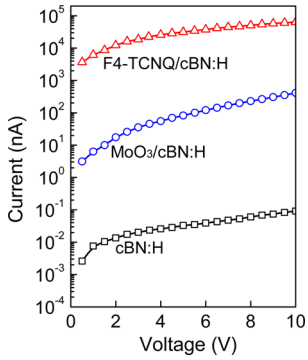

Figure 2. *I*–*V* characteristics acquired from the surface of pristine cBN:H film and after the deposition of 10 nm thick MoO_3 and F4-TCNQ layers.

programmed implantation process using sequential ion energies of 20 to 60 keV was carried out and the total dose was 2.5×10^{15} cm^{-2}. The cBN films were annealed at 1200 °C for 5 min after the ion implantation. The details about ion implantation process can be found elsewhere.[43,44] The resulting modest bulk conductivity enables to eliminate the charging effect during XPS and UPS measurements. The increasing intensities of Mo 3d/3p and F 1s core levels were clearly resolved in the thickness dependent XPS survey spectra (spectra not shown here), corresponding to the accumulated coverages of MoO_3 and F4-TCNQ.

Figure 3 shows the high-resolution XPS spectra of core levels acquired as a function of MoO_3 or F4-TCNQ thicknesses. As presented in Figure 3a, b, the B 1s peak moved toward lower binding energy after MoO_3 or F4-TCNQ were deposited on the surfaces of cBN films. The amplitudes of shift increased with the increase of dopant layer thickness, and finally saturated at 0.4 and 0.6 eV as the thicknesses of MoO_3 and F4-TCNQ layers were over 10 and 2 nm, respectively. Moreover, because the BN stoichiometry at the surface may affect the electronic structure and conductivity of cBN films,[11,13] we also detected B/N ratio by XPS in this study and revealed that it maintained unchanged after the depositions of MoO_3 and F4-TCNQ coatings. Therefore, the observed decrease in binding energy in the XPS spectra suggested the energy decrease in the valence band (VB) of cBN with respect to E_F, i.e., an upward band bending toward the cBN surface. The band bending agreed with the hole accumulation and the resulting built-in potential at the surface of cBN, implying the electron transfer from the VB of cBN to the conduction band (CB) of MoO_3 or to the lowest unoccupied molecular orbital (LUMO) of F4-TCNQ. The holes left in the VB of cBN led to the elevated conductivity at the surface region of cBN films, as revealed in the *I*–*V* measurements. Thus, the transfer of electrons from cBN films to surface acceptors and the enhanced surface conductivity verified the effective p-type surface transfer doping of cBN films.

Further deposition of MoO_3 or F4-TCNQ with thicknesses over 10 and 2 nm, respectively, did not induce further shift of B 1s peak, which suggested that the Fermi levels of cBN and surface dopants reached equilibrium. Similar shifts were also observed for the N 1s core levels in XPS spectra upon the incremental deposition of MoO_3 and F4-TCNQ (spectra not shown here). Because of the strong dielectric screening effect of organic molecules,[45] F4-TCNQ-coated cBN exhibited larger band bending and higher surface conductivity as compared with

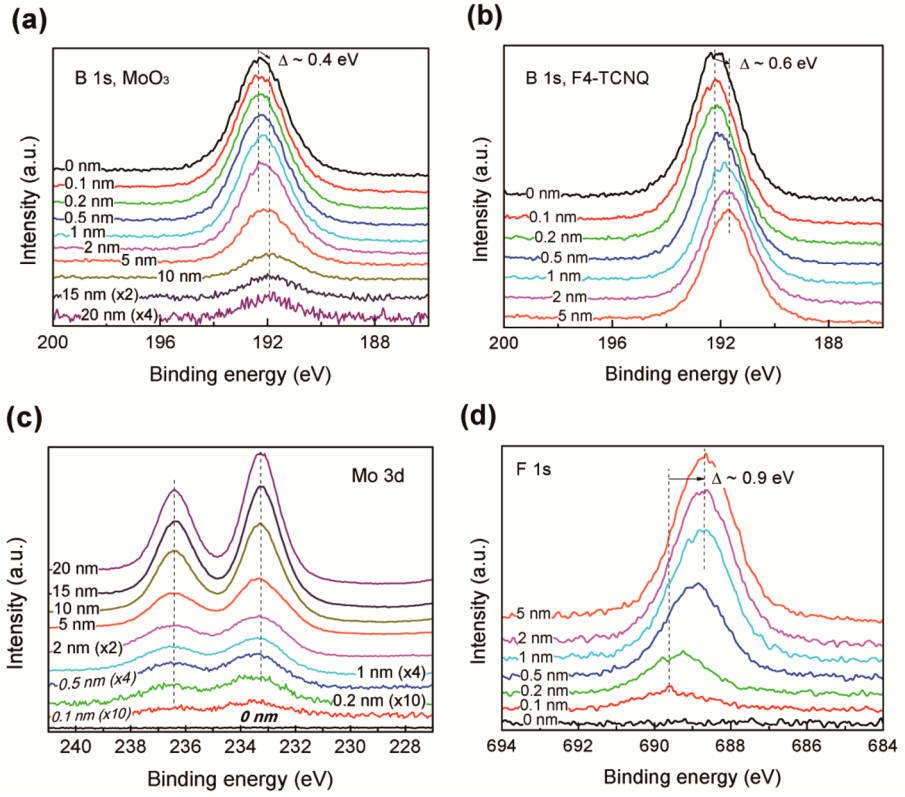

Figure 3. XPS spectra of B 1s core level as a function of (a) MoO_3 and (b) F4-TCNQ thickness. The XPS spectra of (c) Mo 3d and (d) F 1s as a function of thicknesses of MoO_3 and F4-TCNQ, respectively.

DOI: 10.1021/acsami.5b01779
ACS Appl. Mater. Interfaces 2015, 7, 9851–9857

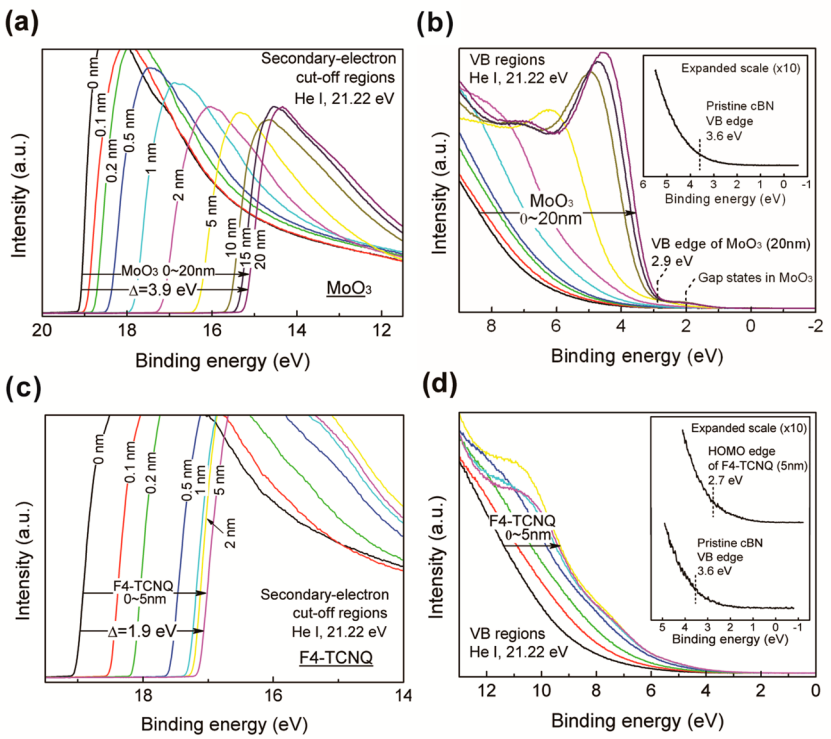

Figure 4. Evolution of (a) work function and (b) VB edge with the increasing coverage of MoO_3 layer on the cBN film. The evolution of (c) work function and (d) VB edge with the increasing coverage of F4-TCNQ layer on the cBN film. The inset in b is the enlarged view of the VB edge of the pristine cBN, and the inset in d presents the enlarged VB edge of pristine cBN and HOMO edge of F4-TCNQ with the thickness of 5 nm.

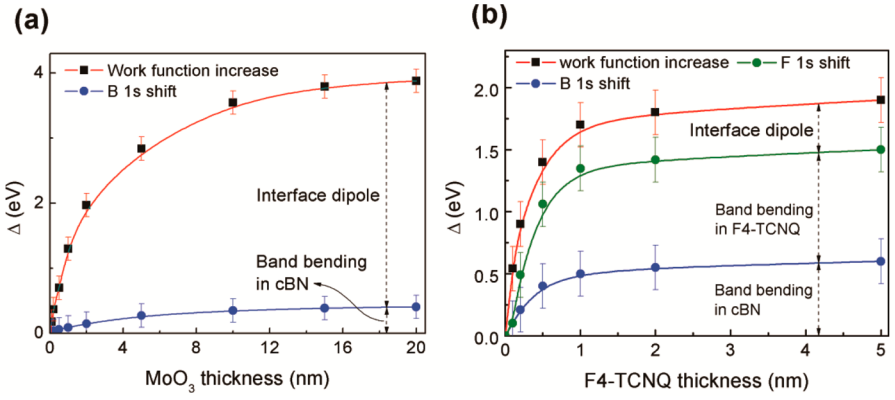

Figure 5. (a) Shift of cBN B 1s peak and the increase in work function as a function of MoO3 thickness. (b) Shifts of cBN B 1s and F4-TCNQ F 1s peaks and the increase in work function as a function of F4-TCNQ thickness.

MoO_3 coated cBN films, suggesting more electrons and holes accumulated at the cBN surface, i.e., a higher doping efficiency of F4-TCNQ. The thickness-dependent high-resolution spectra of Mo 3d and F 1s core levels are shown in Figure 3c, d, respectively. The F 1s peak downshifted more significantly with increasing F4-TCNQ thickness, indicating the energy decrease of the highest occupied molecular orbital (HOMO) with regards to E_F, i.e., a downward band bending toward the cBN surface in the F4-TCNQ coating. In contrast, there was no observable band bending in MoO_3 coatings as seen in Figure 3c.

The series UPS measurements could give a clear view of the electronic structures at the MoO_3/cBN and F4-TCNQ/cBN interfaces. Figure 4 shows the thickness-dependent UPS spectra presenting the evolution of work function and VB at the MoO_3/cBN and F4-TCNQ/cBN interfaces with the incremental deposition of MoO_3 and F4-TCNQ. The secondary-electron cutoff regions in the UPS spectra are shown in Figure 4a, c for MoO_3 and F4-TCNQ coatings, respectively. The work function could be calculated by the equation $\phi = h\nu - E_{SEC}$, where $h\nu$ is 21.22 eV, and E_{SEC} is the secondary electron cutoff, which gives the position of vacuum level. For the pristine cBN film, the work function was 2.1 ± 0.09 eV. With the increasing thicknesses of MoO_3 and F4-TCNQ, the E_{SEC} shifted to lower binding energy which indicated an increase of work function after the deposition of surface dopants. The E_{SEC} shifted by 3.9 eV as the MoO_3 thickness was 20 nm, and for a 5 nm thick F4-TCNQ layer it shifted by 1.9 eV, which corresponded to the work functions of MoO_3 (6.0 ± 0.09 eV) and F4-TCNQ (4.1 ± 0.09 eV), respectively. Figure 4b, d show the evolution of VB regions with the increasing MoO_3 and F4-TCNQ thicknesses. For the pristine cBN film, the onset of VB peak edge was at 3.6

DOI: 10.1021/acsami.5b01779
ACS Appl. Mater. Interfaces 2015, 7, 9851−9857

± 0.09 eV, as depicted in the enlarged plots in Figure 4b, d, illustrating that the VB maximum (VBM) of cBN films located at 3.6 ± 0.09 eV below E_F. The results agree well with the n-type characteristics of Si-doped cBN film with reference to the band gap of cBN films (6.4 eV).[46] As shown in Figure 4b, deposition of 0.1 nm thick MoO_3 layer initiated a clear downshift of VB edge, being consistent with the XPS analysis that bands bended upward at the cBN surface. Subsequent deposition led to the further shift of VB edge. In this case, the VB of cBN could not be resolved from the UPS spectra, thus the VB shift (band bending) of cBN surface had to be estimated by the shift of B 1s core level in XPS spectra. As the thickness of MoO_3 reached 20 nm, the VB peak of MoO_3 centered at 4 eV emerged, and the gap state of MoO_3 due to the oxygen deficiency was also observed at around 2.0 eV.[47,48] The VB edge at 2.9 ± 0.09 eV attributed to MoO_3 could be obtained, which agreed with the previous studies on MoO_3.[49] As presented in Figure 4d, the similar evolution of VB region upon the deposition of F4-TCNQ was revealed. The HOMO edge of F4-TCNQ at 2.7 ± 0.09 eV could be resolved as a 5 nm thick F4-TCNQ layer was coated, being consistent with the reported measurements of F4-TCNQ.[24]

The interfacial charge separation during the surface transfer doping will induce the interface dipole,[50] which in addition to the band bending also contributes to the change of work function. Thus, the interface dipole can be derived by deducting the band bending from the change of work function. As shown in Figure 5a, the increase in work function at MoO_3/cBN interface is plotted as a function of the thickness of MoO_3. The shifts in cBN B 1s peak, which indicate the band bending in cBN are also presented. As seen in the figure, the change of work function is much larger than the shift of cBN B 1s, and the difference enlarges gradually with the increasing MoO_3 coverage and reaches a maximum of 3.55 eV for 20 nm thick MoO_3 because of the formation of interface dipoles. For the F4-TCNQ coating, the shifts of cBN B 1s and F 1s peaks are plotted together with the increase of work function in Figure 5b. The dipoles at F4-TCNQ/cBN interface could be deduced to be 0.4 eV when a 5 nm F4-TCNQ layer was deposited. The much larger interface dipole at MoO_3/cBN interface is due to the higher EA of MoO_3 as compared to that of F4-TCNQ.

On the basis of the PES results, the schematic energy level diagrams before and after the deposition of surface dopants were determined. The band gaps, ionization potentials (IPs) and EAs of MoO_3 and F4-TCNQ were referred to previous studies,[24,27,51] and the band diagram of cBN films was plotted based on its band gap of 6.4 eV.[46] As seen in Figure 6a, c, the CB minimum (CBM) of cBN films was deduced to lie 0.7 eV above the vacuum level (E_{VAC}), which verifies the NEA characteristics of cBN:H surfaces. Due to the large EA of MoO_3, the VBM of cBN lies about 1 eV above the CBM of MoO_3 as referenced to a common E_{VAC} before the deposition. The energy difference drives the electrons to flow from the VB of cBN to the CB of MoO_3 upon the their contact until the equilibrium is reached, which results in the upward band bending with hole accumulation in cBN (Figure 6b). For the F4-TCNQ coating (Figure 6c), the higher E_F of cBN also makes electrons transferred from the VB of cBN to the LUMO of F4-TCNQ, even a small activation barrier exists. As shown in Figure 6d, the LUMO of F4-TCNQ lies below the pinned E_F at its surface because of the band bending in F4-TCNQ, which leads to a strong interaction between cBN and F4-TCNQ. Thus, as compared with the case of MoO_3, more electrons were

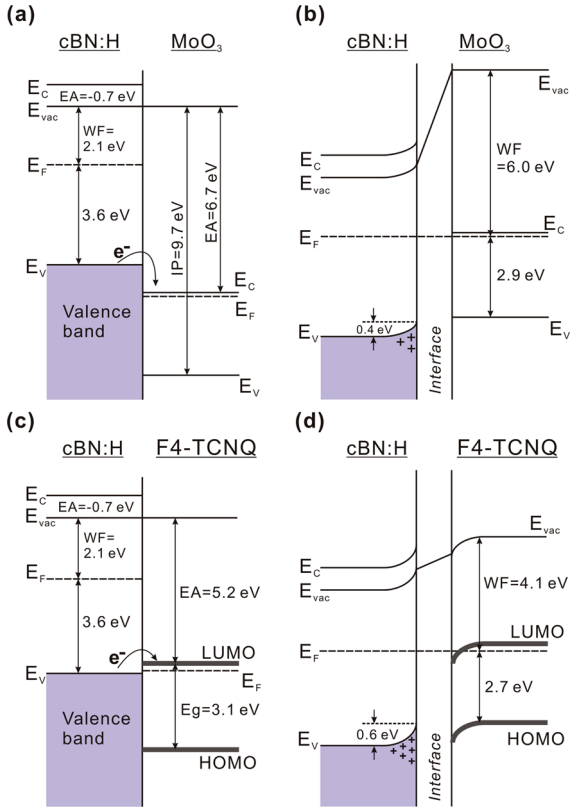

Figure 6. Energy band diagrams before and after the deposition of (a, b) MoO_3 and (c, d) F4-TCNQ, illustrating the surface transfer doping process on cBN:H films. WF represents work function.

transferred to F4-TCNQ and more holes were accumulated at cBN surface. As a result, higher doping efficiency was achieved by using F4-TCNQ. However, considering the thermal and chemical stabilities of these two dopants, MoO_3 may be more attractive in practical applications. Moreover, the low work functions we obtained in this work for MoO_3 and F4-TCNQ (Figure 6b, d) are lower than the previous reports,[24,27] which may be due to the different molecular orientations of F4-TCNQ[18,52] and the thermal reduction of MoO_3 molecules.[49]

CONCLUSIONS

In conclusion, we have demonstrated effective p-type surface transfer doping of cBN:H films by employing MoO_3 and F4-TCNQ as the surface dopants. The surface conductivity of cBN films was enhanced by 3−6 orders in magnification. The PES measurements verified that the large EA difference between cBN and surface dopants drove the electrons to transfer from cBN films to surface acceptors upon their contact. The electronic structures at interfaces were depicted on the basis of the PES results. The interface dipoles and the increase in work function at MoO_3/cBN interface were more significant than that of F4-TCNQ/cBN interface. However, F4-TCNQ was demonstrated to have higher doping efficiency for cBN films. The work provided a new approach to controlling the surface electrical properties of cBN films, which may be favorable for the development of cBN-based electronic devices, especially on micrometer- and nanometer-scales.

AUTHOR INFORMATION

Corresponding Author
*E-mail: apwjzh@cityu.edu.hk.

DOI: 10.1021/acsami.5b01779
ACS Appl. Mater. Interfaces 2015, 7, 9851−9857

Notes

The authors declare no competing financial interest.

■ ACKNOWLEDGMENTS

This work was supported by the grants from the Research Grants Council of the Hong Kong SAR, China (CityU 104911), CityU Strategic Research Grant (SRG 7002725), and National Natural Science Foundation of China (61176007 and 51372213).

■ REFERENCES

(1) Zhang, W. J.; Chong, Y. M.; He, B.; Bello, I.; Lee, S. T. In *Comprehensive Hard Materials*; Sarin, V. K., Nebel, C. E., Eds.; Elsevier: Amsterdam, 2014; Chapter 3.24, pp 607−639.
(2) Wentorf, R. H., Jr. Cubic Form of Boron Nitride. *J. Chem. Phys.* **1957**, *26*, 956.
(3) Wentorf, R. H., Jr. Preparation of Semiconducting Cubic Boron Nitride. *J. Chem. Phys.* **1962**, *36*, 1990.
(4) Mishima, O.; Tanaka, J.; Yamaoka, S.; Fukunaga, O. High-Temperature Cubic Boron Nitride P-N Junction Diode Made at High Pressure. *Science* **1987**, *238*, 181−183.
(5) Mishima, O.; Era, K.; Tanaka, J.; Yamaoka, S. Ultraviolet Light-Emitting Diode of a Cubic Boron Nitride PN Junction Made at High Pressure. *Appl. Phys. Lett.* **1988**, *53*, 962−964.
(6) Mishima, O.; Yamaoka, S.; Fukunaga, O.; Tanaka, J.; Era, K. Cubic Boron Nitride PN Junction Diode Made at High Pressure as a High Temperature Diode and an Ultraviolet LED. In *Science and Technology of New Diamond*; Saito, S., Fukunaga, O., Yoshikawa, M., Eds.; TerraPub: Tokyo, 1990; pp 297−300.
(7) Zhang, W. J.; Chong, Y. M.; Bello, I.; Lee, S. T. Nucleation, Growth and Characterization of Cubic Boron Nitride (cBN) Films. *J. Phys. D: Appl. Phys.* **2007**, *40*, 6159−6174.
(8) Zhang, W. J.; Bello, I.; Lifshitz, Y.; Chan, K. M.; Meng, X. M.; Wu, Y.; Chan, C. Y.; Lee, S. T. Epitaxy on Diamond by Chemical Vapor Deposition: A Route to High-Quality Cubic Boron Nitride for Electronic Applications. *Adv. Mater.* **2004**, *16*, 1405−1408.
(9) Zhang, X. W.; Boyen, H.-G.; Deyneka, N.; Ziemann, P.; Banhart, F.; Schreck, M. Epitaxy of cubic boron nitride on (001)-oriented diamond. *Nat. Mater.* **2003**, *2*, 312−315.
(10) Zhang, X. W. Doping and Electrical Properties of Cubic Boron Nitride Thin Films: A Critical Review. *Thin Solid Films* **2013**, *544*, 2−12.
(11) Kojima, K.; Nose, K.; Kambara, M.; Yoshida, T. Effects of Magnesium Doping on Growth and Electric Conductivity of Nanocrystalline Cubic Boron Nitride Thin Films. *J. Phys. D: Appl. Phys.* **2009**, *42*, 055304.
(12) Nose, K.; Oba, H.; Yoshida, T. Electric Conductivity of Boron Nitride Thin Films Enhanced by in Situ Doping of Zinc. *Appl. Phys. Lett.* **2006**, *89*, 112124.
(13) Nose, K.; Yoshida, T. Semiconducting Properties of Zinc-Doped Cubic Boron Nitride Thin Films. *J. Appl. Phys.* **2007**, *102*, 063711.
(14) Ying, J.; Zhang, X. W.; Yin, Z. G.; Tan, H. R.; Zhang, S. G.; Fan, Y. M. Electrical transport properties of the Si-doped cubic boron nitride thin films prepared by in situ cosputtering. *J. Appl. Phys.* **2011**, *109*, 023716.
(15) He, B.; Zhang, W. J.; Zou, Y. S.; Chong, Y. M.; Ye, Q.; Ji, A. L.; Yang, Y.; Bello, I.; Lee, S. T.; Chen, G. H. Electrical Properties of Be-Implanted Polycrystalline Cubic Boron Nitride Films. *Appl. Phys. Lett.* **2008**, *92*, 102108.
(16) Yin, H.; Pongrac, I.; Ziemann, P. Electronic Transport in Heavily Si Doped Cubic Boron Nitride Films Epitaxially Grown on Diamond(001). *J. Appl. Phys.* **2008**, *104*, 023703.
(17) Ristein, J. Surface Transfer Doping of Semiconductors. *Science* **2006**, *313*, 1057−1058.
(18) Chen, W.; Qi, D. C.; Gao, X. Y.; Wee, A. T. S. Surface Transfer Doping of Semiconductors. *Prog. Surf. Sci.* **2009**, *84*, 279−321.
(19) Lüth, H. *Solid Surfaces, Interfaces and Thin Films*; Springer-Verlag: New York, 2001.
(20) Maier, F.; Riedel, M.; Mantel, B.; Ristein, J.; Ley, L. Origin of Surface Conductivity in Diamond. *Phys. Rev. Lett.* **2000**, *85*, 3472−3475.
(21) Chakrapani, V.; Angus, C. J.; Anderson, B. A.; Wolter, S. D.; Stoner, B. R.; Sumanasekera, G. U. Charge Transfer Equilibria Between Diamond and an Aqueous Oxygen Electrochemical Redox Couple. *Science* **2007**, *318*, 1424−1430.
(22) Zhang, P. P.; Tevaarwerk, E.; Park, B.-N.; Savage, D. E.; Celler, G. K.; Knezevic, I.; Evans, P. G.; Eriksson, M. A.; Lagally, M. G. Electronic Transport in Nanometre-Scale Silicon-on-Insulator Membranes. *Nature* **2006**, *439*, 703−706.
(23) Strobel, P.; Riedel, M.; Ristein, J.; Ley, L. Surface Transfer Doping of Diamond. *Nature* **2004**, *430*, 439−441.
(24) Qi, D. C.; Chen, W.; Gao, X. Y.; Wang, L.; Chen, S.; Loh, K. P.; Wee, A. T. S. Surface Transfer Doping of Diamond (100) by Tetrafluoro-tetracyanoquinodimethane. *J. Am. Chem. Soc.* **2007**, *129*, 8084−8085.
(25) Langley, D. P.; Smets, Y.; Stark, C. B.; Edmonds, M. T.; Tadich, A.; Rietwyk, K. J.; Schenk, A.; Wanke, M.; Wu, Q. H.; Barnard, P. J.; Ley, L.; Pakes, C. I. Surface Transfer Doping of Diamond with a Molecular Heterojunction. *Appl. Phys. Lett.* **2012**, *100*, 032103.
(26) Edmonds, M. T.; Wanke, M.; Tadich, A.; Vulling, H. M.; Rietwyk, K. J.; Sharp, P. L.; Stark, C. B.; Smets, Y.; Schenk, A.; Wu, Q. H.; Ley, L.; Pakes, C. I. Surface Transfer Doping of Hydrogen-Terminated Diamond by $C_{60}F_{48}$ Energy Level Scheme and Doping Efficiency. *J. Chem. Phys.* **2012**, *136*, 124701.
(27) Russell, S. A. O.; Cao, L.; Qi, D. C.; Tallaire, A.; Crawford, K. G.; Wee, A. T. S.; Moran, A. J. Surface Transfer Doping of Diamond by MoO_3. *Appl. Phys. Lett.* **2013**, *103*, 202112.
(28) Chen, W.; Chen, S.; Qi, D. C.; Gao, X. Y.; Wee, A. T. S. Surface Transfer p-Type Doping of Epitaxial Graphene. *J. Am. Chem. Soc.* **2007**, *129*, 10418−10422.
(29) Pinto, H.; Jones, R.; Goss, J. P.; Briddon, P. R. P-Type Doping of Graphene with F4-TCNQ. *J. Phys.: Condens. Matter* **2009**, *21*, 402001.
(30) Chen, Z. Y.; Santoso, I.; Wang, R.; Xie, L. F.; Mao, H. Y.; Huang, H.; Wang, Y. Z.; Gao, X. Y.; Chen, Z. K.; Ma, D.; Wee, A. T. S.; Chen, W. Surface Transfer Hole Doping of Epitaxial Graphene Using MoO_3 Thin Film. *Appl. Phys. Lett.* **2010**, *96*, 213104.
(31) Guo, C. S.; Luo, L. B.; Yuan, G. D.; Yang, X. B.; Zhang, R. Q.; Zhang, W. J.; Lee, S. T. Surface Passivation and Transfer Doping of Silicon Nanowires. *Angew. Chem., Int. Ed.* **2009**, *48*, 9896−9900.
(32) Yuan, G. D.; Zhou, Y. B.; Guo, C. S.; Zhang, W. J.; Tang, Y. B.; Li, Y. Q.; Chen, Z. H.; He, Z. B.; Zhang, X. J.; Wang, P. F.; Bello, I.; Zhang, R. Q.; Lee, C. S.; Lee, S. T. Tunable Electrical Properties of Silicon Nanowires via Surface-Ambient Chemistry. *ACS Nano* **2010**, *4*, 3045−3052.
(33) Yuan, G. D.; Ng, T. W.; Zhou, Y. B.; Wang, F.; Zhang, W. J.; Tang, Y. B.; Wang, H. B.; Luo, L. B.; Wang, P. F.; Bello, I.; Lee, C. S.; Lee, S. T. P-Type Conductivity in Silicon Nanowires Induced by Heterojunction Interface Charge Transfer. *Appl. Phys. Lett.* **2010**, *97*, 153126.
(34) Powers, M. J.; Benjamin, M. C.; Porter, L. M.; Nemanich, R. J.; Davis, R. F.; Cuomo, J. J.; Doll, G. L.; Harris, S. J. Observation of a Negative Electron Affinity for Boron Nitride. *Appl. Phys. Lett.* **1995**, *67*, 3912−3914.
(35) Loh, K. P.; Nishitani-Gamo, M.; Sakaguchi, I.; Taniguchi, T.; Ando, T. Thermal Stability of the Negative Electron Affinity Condition on Cubic Boron Nitride. *Appl. Phys. Lett.* **1998**, *72*, 3023−3025.
(36) Loh, K. P.; Sakaguchi, I.; Nishitani-Gamo, M.; Taniguchi, T.; Ando, T. Negative Electron Affinity of Cubic Boron Nitride. *Diamond Relat. Mater.* **1999**, *8*, 781−784.
(37) Cui, J. B.; Ristein, J.; Ley, L. Electron Affinity of the Bare and Hydrogen Covered Single Crystal Diamond (111) Surface. *Phys. Rev. Lett.* **1998**, *81*, 429−432.
(38) Maier, F.; Ristein, J.; Ley, L. Electron Affinity of Plasma-Hydrogenated and Chemically Oxidized Diamond (100) Surfaces. *Phys. Rev. B* **2001**, *64*, 165411.

DOI: 10.1021/acsami.5b01779
ACS Appl. Mater. Interfaces 2015, 7, 9851−9857

(39) Zhang, W. J.; Chan, C. Y.; Chan, K. M.; Bello, I.; Lifishitz, Y.; Lee, S. T. Deposition of Large-Area, High-Quality Cubic Boron Nitride Films by ECR-Enhanced Microwave-Plasma CVD. *Appl. Phys. A: Mater. Sci. Process.* **2003**, *76*, 953−955.
(40) Zhang, W. J.; Bello, I.; Lifishitz, Y.; Chan, K. M.; Chan, C. Y.; Meng, X. M.; Lee, S. T. Thick and Adherent Cubic Boron Nitride Films Grown on Diamond Interlayers by Fluorine-Assisted Chemical Vapor Deposition. *Appl. Phys. Lett.* **2004**, *85*, 1344−1346.
(41) Zhang, W. J.; Chan, C. Y.; Meng, X. M.; Fung, M. K.; Bello, I.; Lifshitz, Y.; Lee, S. T.; Jiang, X. The Mechanism of Chemical Vapor Deposition of Cubic Boron Nitride Films from Fluorine-Containing Species. *Angew. Chem., Int. Ed.* **2005**, *44*, 4749−4753.
(42) Meng, X. M.; Zhang, W. J.; Chan, C. Y.; Lee, C. S.; Bello, I.; Lee, S. T. Surface Microstructure Analysis of Cubic Boron Nitride Films by TEM. *Appl. Phys. Lett.* **2006**, *88*, 031904.
(43) He, B.; Zhang, W. J.; Yao, Z. Q.; Chong, Y. M.; Yang, Y.; Ye, Q.; Pan, X. J.; Zapien, J. A.; Bello, I.; Lee, S. T.; Gerhards, I.; Zutz, H.; Hofsäss, H. P-Type Conduction in Beryllium-Implanted Hexagonal Boron Nitride Films. *Appl. Phys. Lett.* **2009**, *95*, 252106.
(44) He, B.; Qiu, M.; Yuen, M. F.; Zhang, W. J. Electrical Properties and Electronic Structure of Si-implanted Hexagonal Boron Nitride Films. *Appl. Phys. Lett.* **2014**, *105*, 012104.
(45) Casu, M. B. Evidence for Efficient Screening in Organic Materials. *Phys. Status Solidi RRL* **2008**, *2*, 40−42.
(46) Soltani, A.; Barkad, H.; Mattalah, A. M.; Benbakhti, B.; De Jaeger, J.-C.; Chong, Y. M.; Zou, Y. S.; Zhang, W. J.; Lee, S. T.; BenMoussa, A.; Giordanengo, B.; Hochedez, J.-F. 193 nm deep-ultraviolet solar-blind cubic boron nitride based photodetectors. *Appl. Phys. Lett.* **2008**, *92*, 053501.
(47) Qin, P. L.; Fang, G. J.; Ke, W. J.; Cheng, F.; Zheng, Q.; Wan, J. W.; Lei, H. W.; Zhao, X. Z. In situ Growth of Double-Layer MoO_3/MoS_2 Film from MoS_2 for Hole-Transport Layers in Organic Solar Cell. *J. Mater. Chem. A* **2014**, *2*, 2742−2756.
(48) Kanai, K.; Koizumi, K.; Ouchi, S.; Tsukamoto, Y.; Sakanoue, K.; Ouchi, Y.; Seki, K. Electronic Structure of Anode Interface with Molybdenum Oxide Buffer Layer. *Org. Electron.* **2010**, *11*, 188−194.
(49) Vasilopoulou, M.; Douvas, A. M.; Georgiadou, D. G.; Palilis, L. C.; Kennou, S.; Sygellou, L.; Soultati, A.; Kostis, I.; Papadimitropoulos, G.; Davazoglou, D.; Argitis, P. The Influence of Hydrogenation and Oxygen Vacancies on Molybdenum Oxides Work Function and Gap States for Application in Organic Optoelectronics. *J. Am. Chem. Soc.* **2012**, *134*, 16178−16187.
(50) Ishii, H.; Sugiyama, K.; Ito, E.; Seki, K. Energy Level Alignment and Interfacial Electronic Structures at Organic/Metal and Organic/Organic Interfaces. *Adv. Mater.* **1999**, *11*, 605−625.
(51) Kröger, M.; Hamwi, S.; Meyer, J.; Riedl, T.; Kowalsky, W.; Kahn, A. P-Type Doping of Organic Wide Band Gap Materials by Transition Metal Oxides: A Case-Study on Molybdenum Trioxide. *Org. Electron.* **2009**, *10*, 932−938.
(52) Duhm, S.; Heimel, G.; Salzmann, I.; Glowatzki, H.; Johnson, R. L.; Vollmer, A.; Rabe, J. P.; Koch, N. Orientation-Dependent Ionization Energies and Interface Dipoles in Ordered Molecular Assemblies. *Nat. Mater.* **2008**, *7*, 326−332.

DOI: 10.1021/acsami.5b01779
ACS Appl. Mater. Interfaces 2015, 7, 9851−9857